



Spectral topology and its relation to Fermi arcs in strongly correlated systems

Johan Carlström *Department of Physics, Stockholm University, 106 91 Stockholm, Sweden* (Received 19 January 2023; revised 3 August 2023; accepted 7 August 2023; published 6 September 2023)

Fermi gases and liquids display an excitation spectrum that is simply connected, ensuring closed Fermi surfaces. In strongly correlated systems such as the cuprate superconductors, the existence of open sheets of Fermi surface known as Fermi arcs indicate a distinctly different topology of the spectrum with no equivalent in Fermi-liquid theory. Here, we demonstrate a generic mechanism by which correlation effects in fermionic systems can change the topology of the spectrum. Using diagrammatic Monte Carlo simulations, we demonstrate the existence of disconnected and multiply connected excitation spectra in the attractive Hubbard model in the BCS-BEC crossover regime. These topologically nontrivial spectra are a prerequisite for Fermi arcs.

DOI: [10.1103/PhysRevResearch.5.033160](https://doi.org/10.1103/PhysRevResearch.5.033160)

I. INTRODUCTION

Landau's Fermi-liquid theory [1] is the standard model through which we understand interacting electrons in normal metals. In this paradigm, electronic states evolve adiabatically with increasing interactions so that there remains a direct correspondence between the states in a noninteracting Fermi gas, and the quasiparticles of the interacting system. A key consequence of this relationship is that the excitation spectrum of the interacting system inherits the topology of the bands associated with the noninteracting state. In the absence of gap-closing points, the energy bands of Fermi gases are generally simply connected sets, and so are consequently the spectra of Fermi liquids. This, in turn, implies a Fermi surface that is closed (this point also holds with nodes in the spectrum). Strongly correlated systems often display phenomena that fall decidedly outside of the Fermi-liquid regime. In the cuprates, superconductivity is nucleated from a pseudogap state with open sheets of Fermi surface, which persist over a wide range of doping levels [2]. The physical origin of these Fermi arcs remains highly contested.

It has been observed in the cuprates that superconducting fluctuations persist above the critical temperature [3–5], and it has been proposed that this fact may explain the origin of the pseudogap state [6]. This in turn raises key questions about the pairing regime, which also remains disputed: If the cuprates are BCS-like, then the fluctuating region should be understood in terms of a paired state without global phase coherence [7]. In the BEC limit, the electrons form bound pairs which give rise to a bosonic normal liquid at temperatures far above T_c

[8]. The onset of superconductivity would then occur as these pairs condense at a much lower temperature. While these two scenarios are often both referred to by the term “preformed pairs,” they are remarkably different. Between these two extrema lies an extensive BCS-BEC crossover regime [9].

A directly opposing point of view is that preformed pairs have no part in the emergence of Fermi arcs, and that the pseudogap and paired states are instead antagonistic to each other. Angle-resolved photoemission spectroscopy (ARPES) imaging is claimed to show direct competition between superconductivity, and a distinctly different order parameter that is associated with the pseudogap state [10,11]. A candidate for this order parameter is provided by a breaking of translation symmetry [12], which is observed in scanning tunneling microscopy (STM) imaging [13,14].

Theoretically predicting the existence of Fermi arcs in model Hamiltonians is challenging due to a lack of reliable numerical techniques for strongly correlated fermions. Nonetheless, recent variational Monte Carlo calculations suggest that the pseudogap physics observed in the cuprates is at least qualitatively captured by the single-band Hubbard model. For Hubbard clusters up to 64 sites, Fermi arcs are observed at a carrier concentration of 6.25%, and remnants of these are present at 12.5% doping [15]. This may be compared to the cuprates, where pseudogap physics persist up to a carrier concentration of $\sim 20\%$ [2,16]. The existence of Fermi arcs in a simple model Hamiltonian such as the Hubbard model is encouraging since it may indicate that this is a generic phenomena.

A second theoretical challenge is to qualitatively explain how Fermi-liquid theory fails in strongly correlated systems, and connect this insight with the emergence of Fermi arcs. Here, a key observation is that a simply connected excitation spectrum does not permit open sheets of Fermi surface. This relationship implies that the electronic state's adiabatic dependence on interaction strength must necessarily break down in

Published by the American Physical Society under the terms of the Creative Commons Attribution 4.0 International license. Further distribution of this work must maintain attribution to the author(s) and the published article's title, journal citation, and DOI. Funded by Bibsam.

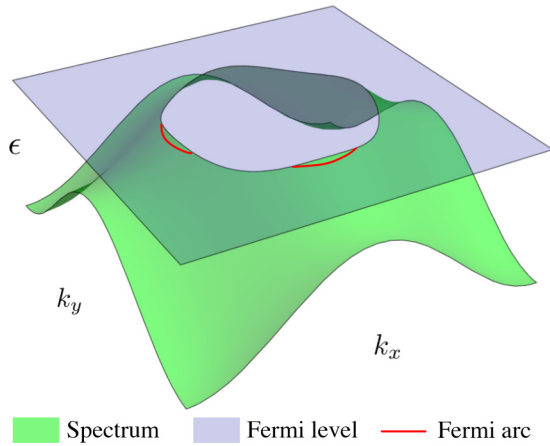


FIG. 1. Relationship between spectral topology and Fermi arcs. The multiply connected spectrum intersects the Fermi level on a set of open and disconnected lines which constitute Fermi arcs. By contrast, a simply connected spectrum must necessarily intersect the Fermi level on a set of closed lines. This implies that a topologically nontrivial spectrum is a prerequisite of Fermi arcs.

such a way that the connectivity of the spectrum changes (see also Fig. 1).

In this paper, we discuss how strong interactions can give rise to non-Fermi-liquid phases which are characterized by band fractionalization [17]. Using the attractive-interaction Hubbard model as an example, we demonstrate that the operators associated with these fractional bands exhibit vanishing phase spaces in parts of the Brillouin zone, which leads to disconnected or multiply connected excitation spectra. These topologically nontrivial spectra are a fundamental prerequisite for the existence of Fermi arcs.

II. BAND FRACTIONALIZATION AND SPECTRAL TOPOLOGY

To illustrate the breakdown of Fermi-liquid theory, we consider the attractive Hubbard model (AHM), which is given by

$$H = \sum_{(ij)\sigma} t c_{i\sigma}^\dagger c_{j\sigma} + \sum_i (U n_{i\downarrow} n_{i\uparrow} - \mu n_i), \quad U < 0. \quad (1)$$

Because of the interaction, the energy bands are generally split into two subbands, [18], a phenomenon that is also referred to as band fractionalization [17]. For a strong contact interaction, these subbands are generally singlonlike and doublonlike, respectively, prompting us to introduce the corresponding operators and associated spinors:

$$\begin{aligned} c_{i\sigma}^\dagger &= s_{i\sigma}^\dagger + d_{i\sigma}^\dagger, & s_{i\sigma}^\dagger &= c_{i\sigma}^\dagger (1 - n_{i\bar{\sigma}}), & d_i^\dagger &= c_{i\sigma}^\dagger n_{i\bar{\sigma}}, \\ \Psi_{i\sigma}^\dagger &= [s_{i\sigma}^\dagger \ d_{i\sigma}^\dagger], & \Psi_{i\sigma} &= \begin{bmatrix} s_{i\sigma} \\ d_{i\sigma} \end{bmatrix}. \end{aligned} \quad (2)$$

Here, s^\dagger and d^\dagger are the singlon and doublon creation operators while $\bar{\sigma} = -\sigma$. We can then define a “quasiparticle” (QP) Green’s function based on the outer product of the spinors,

$$\Gamma_\sigma(x_2 - x_1) = \langle T_\tau \Psi_{i\sigma}^\dagger(x_1) \otimes \Psi_{i\sigma}(x_2) \rangle, \quad (3)$$

from which the ordinary electronic Green’s function is obtained by the summation

$$G_\sigma(x) = \sum_{\alpha\beta} \Gamma_{\alpha\beta\sigma}(x). \quad (4)$$

In the atomic limit, the QP Green’s function is diagonal, with a frequency space representation given by

$$\Gamma_\sigma^A(\omega) = \begin{bmatrix} \frac{1+e^\mu}{Z_A} \frac{1}{i\omega+\mu} & 0 \\ 0 & \frac{e^\mu+e^{2\mu-U}}{Z_A} \frac{1}{i\omega+\mu-U} \end{bmatrix}. \quad (5)$$

Here, the energy is for simplicity given in units of the temperature (corresponding to the case of unit temperature). The Green’s function (5) resembles that of a two-component system, except that it is rescaled by two “quasiparticle weights.” To pursue this analogy we introduce the weight W according to

$$W = \begin{bmatrix} \frac{1+e^\mu}{Z_A} & 0 \\ 0 & \frac{e^\mu+e^{2\mu-U}}{Z_A} \end{bmatrix} = w_0 \sigma_0 + w_z \sigma_z, \quad (6)$$

where we note that (6) must satisfy

$$w_0 \geq |w_z|. \quad (7)$$

In the limit $w_z \rightarrow w_0$, the system is effectively Gutzwiller projected, and doublons can be regarded as “forbidden.” In this scenario, the doublon operators can be said to have a vanishing phase space in the sense that they have a domain or codomain which does not overlap with the subspace on which we project. The same can be said about the singlon operator in the limit $w_z \rightarrow -w_0$. In these cases, the doublon or singlon parts do not contribute to the Green’s function, and thus not to the spectrum either.

We may then express the atomic Green’s function (5) in terms of a reweighted two-component system according to

$$\Gamma_\sigma^A(\omega) = \frac{W}{i\omega - V}, \quad V = \left[\frac{U}{2} - \mu \right] \sigma_0 - \frac{U}{2} \sigma_z, \quad (8)$$

where V is the effective two-component Hamiltonian.

Next, we note that the tunneling term may be written

$$t c_{i\sigma}^\dagger c_{j\sigma} = \Psi_{i\sigma}^\dagger K \Psi_{j\sigma}, \quad K = t(\sigma_0 + \sigma_x). \quad (9)$$

Thus, including the first correction of the strong-coupling expansion [19], we obtain a Green’s function

$$\begin{aligned} \Gamma_\sigma(\omega) &= \Gamma_\sigma^A(\omega) + \Gamma_\sigma^A(\omega) K(\mathbf{k}) \Gamma_\sigma^A(\omega) + \dots \\ &= \frac{1}{i\omega - V - WK(\mathbf{k})} W. \end{aligned} \quad (10)$$

At this point, the effective two-component Hamiltonian $H_e = V + WK(\mathbf{k})$ is no longer diagonal, and the dispersion thus mixes the singlon and doublon components. Additionally, H_e is non-Hermitian, and does not generally exhibit an orthonormal eigenbasis. However, due to a combination of \mathcal{PT} symmetry and the condition (7), the eigenvalues remain real.

Due to the factor W , the spectral weights of the two subbands are generally not equal, and one of them may even vanish asymptotically. This point is central to the spectral topology: If we conduct a strong-coupling expansion to higher

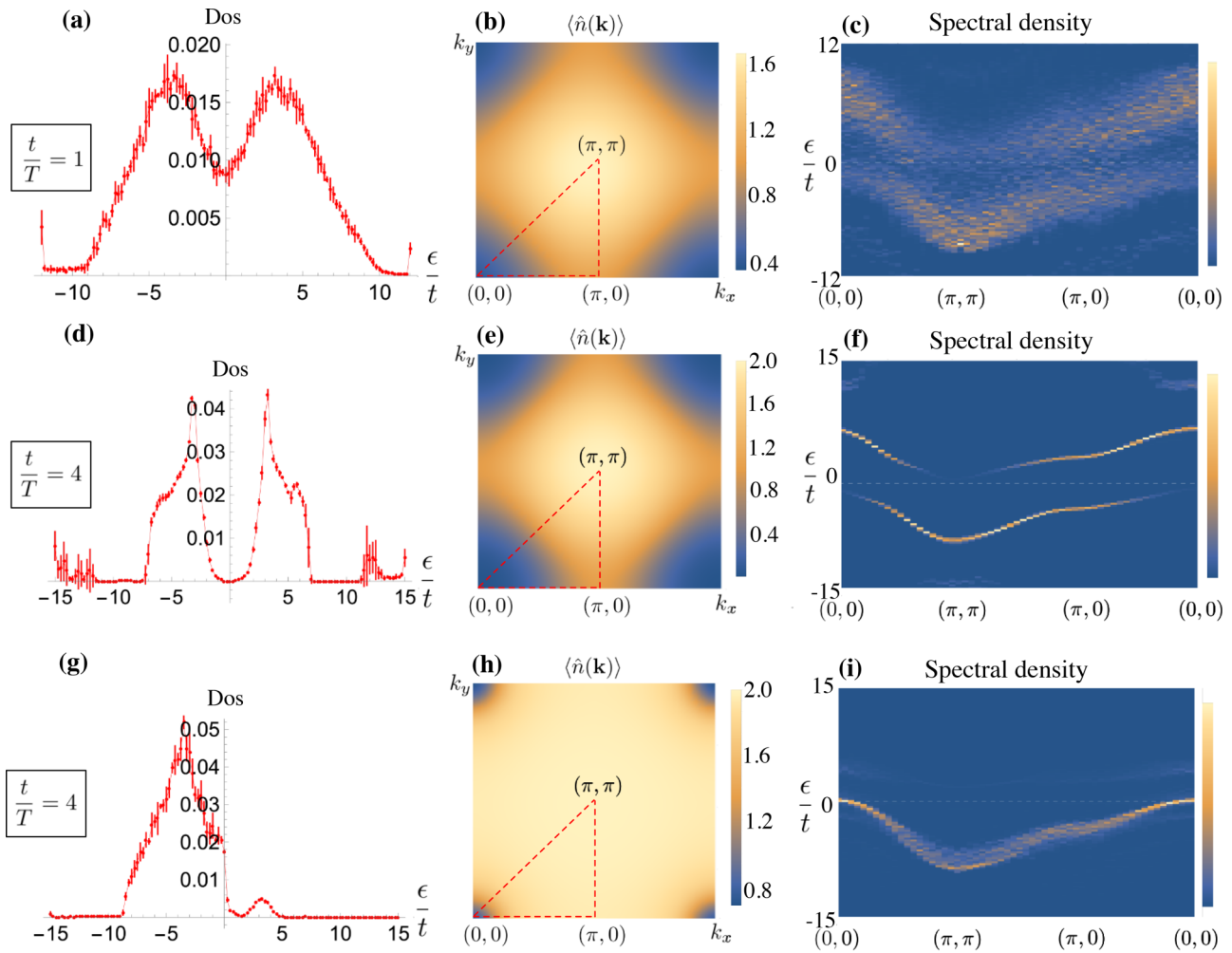


FIG. 2. Spectra and equation of state for the attractive Hubbard model with $U = -5|t|$, at temperatures of (a)–(c) $t/T = 1$ and (d)–(i) $t/T = 4$. (a)–(f) correspond to half filling, while (g)–(i) correspond to $\langle \hat{n} \rangle \approx 1.88$. At high temperature, the spectrum (a) reveals a suppression of the density of states at the Fermi level. The particle density (b) exhibits a minimum at $\mathbf{k} = (0, 0)$ with $\langle \hat{n} \rangle \approx 0.4$ and a maximum at $\mathbf{k} = (\pi, \pi)$ with $\langle \hat{n} \rangle \approx 1.6$. The momentum-resolved spectral density (c) taken along the dashed line in (b) reveals two subbands. Decreasing the temperature, the density of states (d) vanishes at the Fermi level, implying that the system is gapped with respect to fermionic excitations. The particle density (e) now has minima and maxima close to 0 and 2.0, respectively. The spectral density (f) reveals sharp families of excitations with a spectral weight that is strongly dependent on momentum and almost vanishes in part of the Brillouin zone. Increasing the particle density to $\langle \hat{n} \rangle \approx 1.88$, the density of states (g) reveals a large peak that is doublonlike, and a much suppressed peak corresponding to singlons. The peaks are well separated, and the density of states vanishes at $\epsilon \approx 1.5t$. The spectral density reveals a large doublonlike peak, though the singlon peak has a presence mainly near $\mathbf{k} = (0, 0)$. This data were obtained using an expansion order $O = 6$.

order, then we will find that the QP weight W becomes momentum dependent. If the phase space for a subband operator of the type (2) vanishes in part of the Brillouin zone, then so does the corresponding spectral weight, implying that the spectrum is no longer simply connected.

The principal mechanism behind this phenomenon transpires from Eq. (2): In contrast to fermionic operators, the QP operators effectively contain projections onto a subspace of the Hilbert space. For a particle density satisfying $\langle n(\mathbf{k}) \rangle = 0$ we must have that the operators $d_{\mathbf{k},\sigma}^\dagger, d_{\mathbf{k},\sigma}$ both vanish when acting on this state, implying that the corresponding component of the QP Green's function in Eq. (3) is zero, along with

the related spectral density. The same occurs for the singlon pair $S_{\mathbf{k},\sigma}^\dagger, S_{\mathbf{k},\sigma}$ when $\langle n(\mathbf{k}) \rangle = 2$.

Strong-coupling expansion by hand is however not feasible beyond first order, and to explore this concept we have to employ numerical techniques.

III. NUMERICAL TREATMENT

To test the preceding conjecture, we employ bold-line diagrammatic Monte Carlo simulations, specifically focusing on the attractive Hubbard model in the BCS-BEC crossover regime [20–23]. This method is based on the stochastic

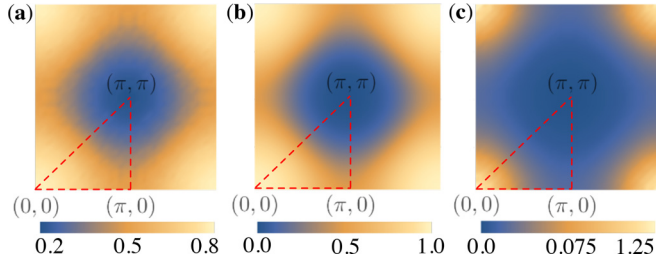


FIG. 3. Spectral weight of the singlonlike subband, obtained from Eq. (16). At half filling and a temperature of $t/T = 1$ (a), the weight is suppressed near $\mathbf{k} = (\pi, \pi)$ and reaches a minimum of $\approx 16\%$. Reducing the temperature (b), this minimum approaches zero. Consequently, the set of points in momentum space where this quasiparticle family has a finite spectral weight is now multiply connected. Increasing the particle density to $\langle \hat{n} \rangle \approx 1.88$ (c), the spectrum retains a finite weight near $\mathbf{k} = (0, 0)$ but almost vanishes elsewhere, thus becoming disconnected. The strong suppression of the spectral weight at certain momenta can be understood from a vanishing phase space of singlonlike excitations.

sampling of Feynman-type graphs [24], and is unbiased in the sense that the only systematic source of error is truncation of the series. For a convergent series, asymptotically exact results are obtained directly in the macroscopic limit. To be able to address systems with strong interactions we use a particular formulation known as strong-coupling diagrammatic Monte Carlo (SCDMC) [19,25–28], where the diagrammatic elements are connected vertices of propagating electrons that are nonperturbative in U . The computational protocol employed here is outlined in detail in Ref. [19].

In SCDMC, the expansion parameter is the hopping integral t . The principal observable that we compute is the polarization operator of the hopping integral, here denoted $\Pi_t(\omega, \mathbf{k})$. From the polarization operator, we obtain the dressed hopping integral via the Bethe-Salpeter equation

$$\tilde{t}(\omega, \mathbf{k}) = \frac{1}{t^{-1}(\mathbf{k}) - \Pi_t(\omega, \mathbf{k})}. \quad (11)$$

We expand in the dressed hopping \tilde{t} , while retaining only the skeleton diagrams. By iterating until convergence, we obtain a self-consistent solution for \tilde{t} which implicitly takes into account certain classes of diagrams to infinite order.

The Green's function of the interacting system is closely related to the dressed hopping integral, and can be obtained from the equation

$$G(\omega, \mathbf{k}) = \frac{1}{\Pi_t^{-1}(\omega, \mathbf{k}) - t_{\mathbf{k}}}. \quad (12)$$

To the lowest order, the polarization operator is given by the atomic-limit Green's function, meaning that Eq. (10) is reproduced. We conduct a self-consistent summation of all diagrams to order 7 which permits us to assess convergence properties of the series—for a discussion, see the Appendix.

We compute a discrete approximation for the spectrum using a numerical analytical continuation protocol [29]: First, we define a spectral reconstruction of the Green's function and a corresponding error metric according to

$$G_R(\tau, \mathbf{k}) = \sum_{n=1}^{n_{\max}} A_n(\mathbf{k}) \frac{e^{-\epsilon_n \tau}}{1 + e^{\beta \epsilon_n}}, \quad \tau < 0, \quad (13)$$

$$\Delta[\mathbf{k}, \{A_n(\mathbf{k})\}] = \sqrt{\frac{1}{\beta} \int d\tau [G(\tau, \mathbf{k}) - G_R(\tau, \mathbf{k})]^2}. \quad (14)$$

We use $n_{\max} = 121$ as a compromise between accuracy and computational cost. To obtain the best estimate for the spectral function $A(\mathbf{k})$, we minimize the error metric Δ through a process of simulated annealing followed by a line-search technique: In the first stage, we use Monte Carlo to update $\{A_n(\mathbf{k})\}$ with an acceptance ration $\sim e^{-\kappa \Delta}$, while successively increasing the inverse pseudotemperature κ . In the second stage, we minimize Δ using Newton-Raphson. This reduces the error only very slightly, but tends to result in a smoother spectrum.

From the spectrum, we obtain a (discretized) estimate for the density of states via the integral

$$\text{DOS}(\epsilon_n) = \int \frac{d\mathbf{k}}{(2\pi)^D} A_n(\mathbf{k}). \quad (15)$$

The normalization of Eq. (13) is such that the summations over A_n and $\text{DOS}(\epsilon_n)$ are unity.

We consider the Hubbard model with an attractive contact interaction given by $U = -5|t|$, at temperatures $t/T = 1$ and $t/T = 4$. This parameter choice ensures that the attraction is strong enough to suppress fermionic degrees of freedom near the Fermi level. Stronger attraction would only enhance this effect. We examine the cases of half filling and a particle density of $\langle \hat{n} \rangle \approx 1.88$. The results of our simulations are summarized in Fig. 2.

At half filling and a higher temperature of $t/T = 1$, we find that the density of states [Fig. 2(a)] has a minimum at the Fermi level, though the system remains gapless. The momentum-resolved particle density [Fig. 2(b)] attains minima and maxima at ~ 0.4 and ~ 1.6 . The spectral density [Fig. 2(c)] exhibits two smeared subbands, with densities that are visibly momentum dependent.

Reducing the temperature, the density of states [Fig. 2(d)] vanishes at the Fermi level, indicating that the system is gapped against fermionic excitations. The particle density extrema [Fig. 2(e)] are now close to 0 and 2.0, respectively. The spectral density [Fig. 2(f)] is sharply peaked, with a weight that is strongly dependent on momentum.

If we also increase the particle density, then the upper subband is strongly suppressed as a result [Fig. 2(g)]. The system is now completely filled in a large fraction of the Brillouin zone [Fig. 2(h)], and the lower subband carries most of the spectral weight [Fig. 2(i)].

The momentum-dependent spectral weights can be understood from the fact that the two subbands originate in singlonlike and doublonlike degrees of freedom: For a sufficiently strong attraction, the Hubbard model prefers to have occupation numbers of 0 or 2. Singly occupied sites are situated at high energy, implying that the upper subband is singlonlike. At small momenta, $\mathbf{k} \approx (0, 0)$, the particle density is smaller, and the singlon operator has a substantial phase space allowing for a high spectral density. Near $\mathbf{k} = (\pi, \pi)$, the particle density approaches 2, meaning that the phase space for the singlon operator vanishes, along with the spectral weight of this subband. For the doublonlike component, the situation is the opposite, with a vanishing spectral density when the density is small.

To quantify the suppression of the spectral density, we define the spectral weight of a subband according to

$$\rho(\mathbf{k}) = \sum_{n=n_{\min}}^{n=n_{\max}} A_n(\mathbf{k}), \quad (16)$$

where the range of indices n should be taken to include the entire subband, but nothing else. At a temperature of $t/T = 4$ and half filling, the system remains gapped so that we can identify the upper subband with positive energies and the lower subband with negative energies. Doping the system, the two subbands are still well separated with the density of states vanishing at $\epsilon \approx 1.5t$, suggesting we use this energy as the dividing point. At the higher temperature, the two subbands overlap. We can still calculate spectral weights based on $\epsilon = 0$ as our dividing point, though this approximation may slightly underestimate the spectral weight at its minimum, while overestimating it at the maximum.

The spectral weight of the singlonlike component is shown in Fig. 3. At a temperature of $t/T = 1$ and half filling [Fig. 3(a)], the singlonlike component is suppressed to $\approx 16\%$ at $\mathbf{k} \approx (\pi, \pi)$. At a temperature of $t/T = 4$ [Fig. 3(b)], this minimum drops below 1%. The strong temperature dependence is consistent with the notion of a vanishing phase space for the singlon operator: At $\mathbf{k} = (\pi, \pi)$, the system has a preference for double occupation, and the singlon operator can only act in the presence of thermal fluctuations. As the temperature is reduced, these are exponentially suppressed together with the spectral weight. Asymptotically, this results in a family of quasiparticles which only has a finite spectral weight in part of the Brillouin zone, and thus a multiply connected spectrum. Increasing the particle density [Fig. 3(c)], the spectral weight attains a maximum at $\mathbf{k} = (0, 0)$ while asymptotically vanishing between these. The result is a disconnected spectrum.

It should be noted that we do not reach the point where the spectrum completely vanishes since we are limited to finite temperatures. Diagrammatic Monte Carlo generally requires that the series converges, and this is often not the case at sufficiently low temperatures. Real condensed-matter systems are also generally realized at finite temperature. However, thermal fluctuations are exponentially suppressed with the inverse temperature. If the relevant energy scale is large compared to the temperature, then we can for all practical purposes regard the systems as being in the asymptotic limit where the spectral density vanishes in part of the Brillouin zone.

Once the spectrum has a nontrivial connectivity, there are no topological obstacles to an intersection with the Fermi level that is an open line in two dimensions (2D), as shown in Fig. 1, or an open surface in 3D.

IV. CONCLUSIONS

In non-Fermi liquids, band fractionalization effectively splits the electron energy into a distribution of quasiparticle energies. The spectral weight of these subbands is determined by the phase space of the corresponding operators, implying that it is generally momentum dependent. In strongly correlated systems, this phase space may—to exponential accuracy—vanish, creating voids in parts of the Brillouin zone which change the topology of the excitation spectrum. This effect is a prerequisite for Fermi arcs, and spectral topology should therefore be regarded as an essential property of strongly correlated phases.

ACKNOWLEDGMENTS

This work was supported by the Swedish Research Council (VR) through Grant No. 2018-03882. Computations were performed on resources provided by the Swedish National Infrastructure for Computing (SNIC) at the National Supercomputer Centre in Linköping, Sweden.

APPENDIX

To assess how truncation of the series affects the results, we compare the density of states and spectral function for the cases reported in the paper at different expansion orders. In Fig. 4 we show the case of half filling and temperatures $t/T = 1$ and $t/T = 4$ for expansion orders $O = 5, 6, 7$. At the higher temperature, we observe that the DOS changes very little, though a small correction at $\epsilon = 0$ is visible. The spectrum is qualitatively very similar, and we conclude that the impact of truncation is very small.

At the lower temperature, we see some changes in the shape of the DOS when increasing the order from 5 to 6, though the system consistently remains gapped. The spectra show a weight that does not completely vanish at $O = 5$, but is strongly suppressed at higher orders. At $O = 7$, we begin to see noise in the spectrum as a result of the computational cost associated with expansions to high order. For this data set, we can conclude that truncation of the series has a limited quantitative impact, but it does not affect any of the conclusions derived in the paper.

In Fig. 5, we see the DOS and spectra for the doped case at expansion orders $O = 5, 6, 7$. In this scenario, truncation of the series has no impact visible to the naked eye, and we can conclude that the result is virtually exact.

In conclusion, we find that the diagrammatic Monte Carlo simulations reported do accurately capture the physics of the attractive Hubbard model. The results are qualitatively not affected by a truncation of the series, yet a small quantitative uncertainty remains for one of the data sets.

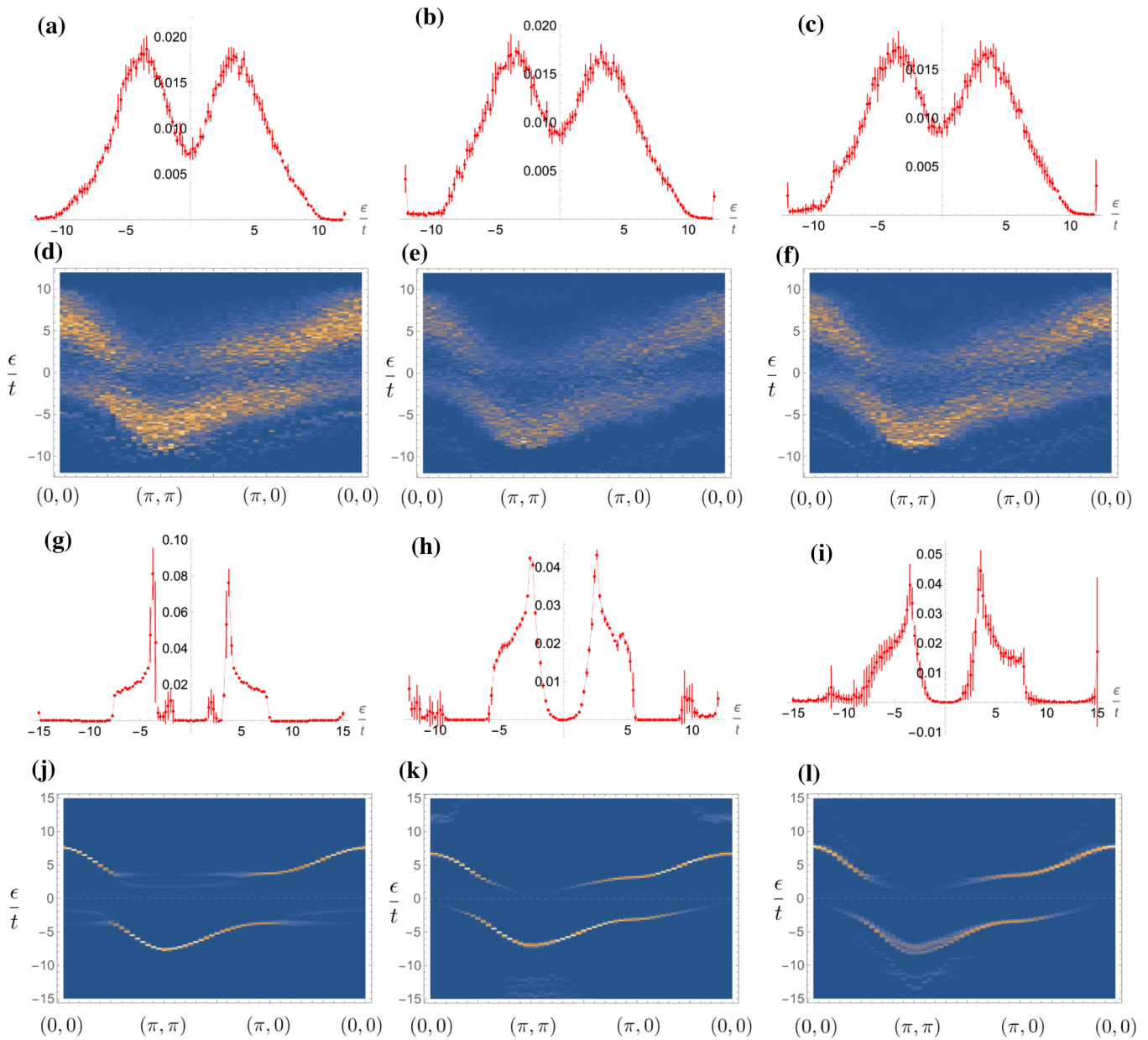


FIG. 4. Convergence of the series at half filling. The left column corresponds to an expansion order $O = 5$, the center corresponds to $O = 6$, and the right corresponds to $O = 7$. (a)–(c) give the DOS at a temperature of $t/T = 1$, while (d)–(f) give the corresponding spectra. (g)–(i) give the DOS at a temperature of $t/T = 4$, while (j)–(l) give the corresponding spectra. At the higher temperature, the corrections when changing the expansion order are very small, though a slight shift in DOS at the Fermi level can be observed when comparing (a) $O = 5$ and (b) $O = 6$. At the lower temperature, we do see a quantitative difference in DOS between (g) orders 5 and (h) 6 while the correction at (i) order 7 is smaller. The small peaks in the DOS near the Fermi level in (g) are reflected in a suppressed fractionalized subband visible in (j). At orders 6 and 7, this fractionalized subband vanishes.

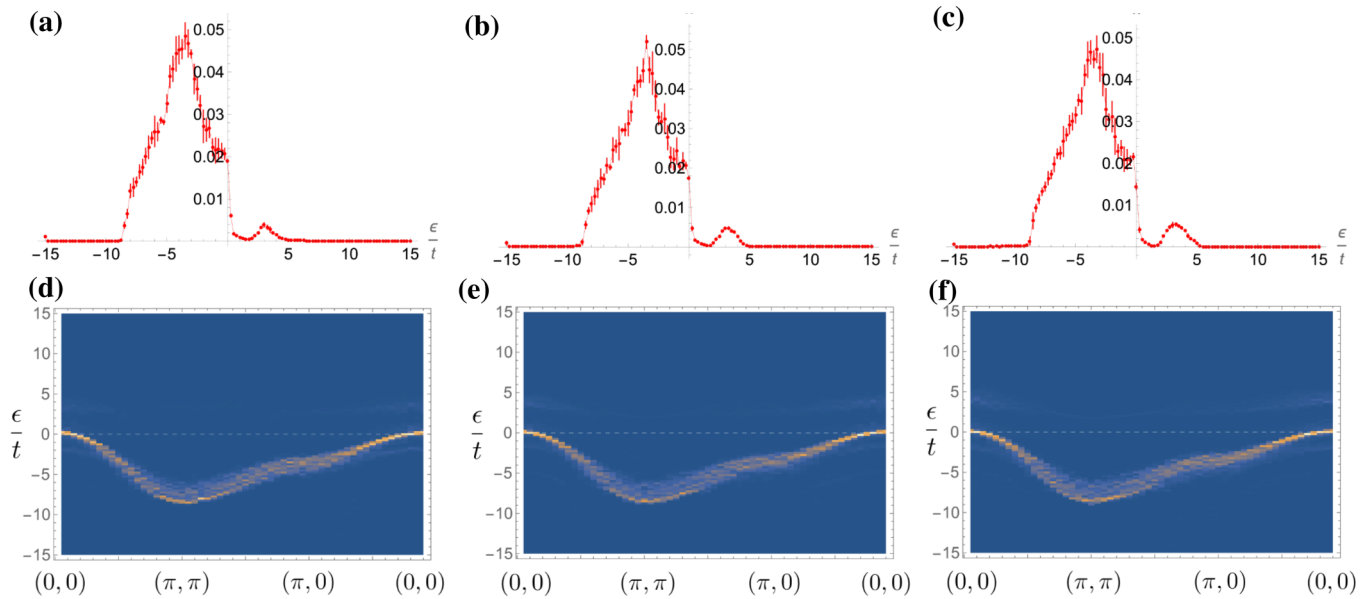


FIG. 5. Convergence of the series in the strongly doped case. The density is $\langle \hat{n} \rangle \approx 1.88$ and the temperature is $t/T = 4$. The left column [(a), (d)] corresponds to an expansion order $O = 5$, the center column to $O = 6$, and the right columns to $O = 7$. The DOS [(a)–(c)] does not change visibly with expansion order, and neither does the spectrum [(d)–(f)]. We can therefore conclude that the observables have converged.

- [1] L. D. Landau, E. M. Lifshitz, and L. P. Pitaevskii, *Course of Theoretical Physics: Statistical Physics, Part 2: by E. M. Lifshitz and L. P. Pitaevskii*, Vol. 9 (Pergamon, Oxford, UK, 1980).
- [2] S.-D. Chen, M. Hashimoto, Y. He, D. Song, K.-J. Xu, J.-F. He, T. P. Devereaux, H. Eisaki, D.-H. Lu, J. Zaanen, and Z.-X. Shen, Incoherent strange metal sharply bounded by a critical doping in Bi2212, *Science* **366**, 1099 (2019).
- [3] T. Kondo, W. Malaeb, Y. Ishida, T. Sasagawa, H. Sakamoto, T. Takeuchi, T. Tohyama, and S. Shin, Point nodes persisting far beyond T_c in Bi2212, *Nat. Commun.* **6**, 7699 (2015).
- [4] Y. He, S.-D. Chen, Z.-X. Li, D. Zhao, D. Song, Y. Yoshida, H. Eisaki, T. Wu, X.-H. Chen, D.-H. Lu, C. Meingast, T. P. Devereaux, R. J. Birgeneau, M. Hashimoto, D.-H. Lee, and Z.-X. Shen, Superconducting fluctuations in overdoped Bi₂Sr₂CaCu₂O_{8+δ}, *Phys. Rev. X* **11**, 031068 (2021).
- [5] N. Bergeal, J. Lesueur, M. Aprili, G. Faini, J. P. Contour, and B. Leridon, Pairing fluctuations in the pseudogap state of copper-oxide superconductors probed by the Josephson effect, *Nat. Phys.* **4**, 608 (2008).
- [6] Y. I. Seo, W. J. Choi, S.-i. Kimura, and Y. S. Kwon, Evidence for a preformed Cooper pair model in the pseudogap spectra of a Ca₁₀(Pt₄As₈)(Fe₂As₂)₅ single crystal with a nodal superconducting gap, *Sci. Rep.* **9**, 3987 (2019).
- [7] J. Sous, Y. He, and S. A. Kivelson, Absence of a BCS-BEC crossover in the cuprate superconductors, [arXiv:2210.13478](https://arxiv.org/abs/2210.13478).
- [8] S. Jiang, L. Zou, and W. Ku, Non-Fermi-liquid scattering against an emergent Bose liquid: Manifestations in the kink and other exotic quasiparticle behavior in the normal-state cuprate superconductors, *Phys. Rev. B* **99**, 104507 (2019).
- [9] N. Harrison and M. K. Chan, Magic Gap Ratio for Optimally Robust Fermionic Condensation and its Implications for High- T_c Superconductivity, *Phys. Rev. Lett.* **129**, 017001 (2022).
- [10] M. Hashimoto, R.-H. He, K. Tanaka, J.-P. Testaud, W. Meevasana, R. G. Moore, D. Lu, H. Yao, Y. Yoshida, H. Eisaki, T. P. Devereaux, Z. Hussain, and Z.-X. Shen, Particle-hole symmetry breaking in the pseudogap state of Bi2201, *Nat. Phys.* **6**, 414 (2010).
- [11] M. Hashimoto, E. A. Nowadnick, R.-H. He, I. M. Vishik, B. Moritz, Y. He, K. Tanaka, R. G. Moore, D. Lu, Y. Yoshida, M. Ishikado, T. Sasagawa, K. Fujita, S. Ishida, S. Uchida, H. Eisaki, Z. Hussain, T. P. Devereaux, and Z.-X. Shen, Direct spectroscopic evidence for phase competition between the pseudogap and superconductivity in Bi₂Sr₂CaCu₂O_{8+δ}, *Nat. Mater.* **14**, 37 (2015).
- [12] J.-H. Ma, Z.-H. Pan, F. C. Niestemski, M. Neupane, Y.-M. Xu, P. Richard, K. Nakayama, T. Sato, T. Takahashi, H.-Q. Luo, L. Fang, H.-H. Wen, Z. Wang, H. Ding, and V. Madhavan, Coexistence of Competing Orders with Two Energy Gaps in Real and Momentum Space in the High Temperature Superconductor Bi₂Sr_{2-x}La_xCuO_{6+δ}, *Phys. Rev. Lett.* **101**, 207002 (2008).
- [13] W. D. Wise, M. C. Boyer, K. Chatterjee, T. Kondo, T. Takeuchi, H. Ikuta, Y. Wang, and E. W. Hudson, Charge-density-wave origin of cuprate checkerboard visualized by scanning tunnelling microscopy, *Nat. Phys.* **4**, 696 (2008).
- [14] J. E. Hoffman, E. W. Hudson, K. M. Lang, V. Madhavan, H. Eisaki, S. Uchida, and J. C. Davis, A four unit cell periodic pattern of quasi-particle states surrounding vortex cores in Bi₂Sr₂CaCu₂O_{8+δ}, *Science* **295**, 466 (2002).
- [15] P. Rosenberg, D. Sénéchal, A.-M. S. Tremblay, and M. Charlebois, Fermi arcs from dynamical variational Monte Carlo, *Phys. Rev. B* **106**, 245132 (2022).

- [16] S. Badoux, W. Tabis, F. Laliberté, G. Grissonnanche, B. Vignolle, D. Vignolles, J. Béard, D. A. Bonn, W. N. Hardy, R. Liang, N. Doiron-Leyraud, L. Taillefer, and C. Proust, Change of carrier density at the pseudogap critical point of a cuprate superconductor, *Nature (London)* **531**, 210 (2016).
- [17] M. Imada and T. J. Suzuki, Excitons and dark fermions as origins of Mott gap, pseudogap and superconductivity in cuprate superconductors - general concept and basic formalism based on gap physics, *J. Phys. Soc. Jpn.* **88**, 024701 (2019).
- [18] K. A. Chao, J. Spałek, and A. M. Oleś, Canonical perturbation expansion of the Hubbard model, *Phys. Rev. B* **18**, 3453 (1978).
- [19] J. Carlström, Strong-coupling diagrammatic Monte Carlo technique for correlated fermions and frustrated spins, *Phys. Rev. B* **103**, 195147 (2021).
- [20] R. T. Scalettar, E. Y. Loh, J. E. Gubernatis, A. Moreo, S. R. White, D. J. Scalapino, R. L. Sugar, and E. Dagotto, Phase diagram of the two-dimensional negative- U Hubbard model, *Phys. Rev. Lett.* **62**, 1407 (1989).
- [21] A. Moreo and D. J. Scalapino, Two-dimensional negative- U Hubbard model, *Phys. Rev. Lett.* **66**, 946 (1991).
- [22] T. Paiva, R. R. dos Santos, R. T. Scalettar, and P. J. H. Denteneer, Critical temperature for the two-dimensional attractive Hubbard model, *Phys. Rev. B* **69**, 184501 (2004).
- [23] J. E. Hirsch, Two-dimensional Hubbard model: Numerical simulation study, *Phys. Rev. B* **31**, 4403 (1985).
- [24] K. Van Houcke, E. Kozik, N. Prokof'ev, and B. Svistunov, Diagrammatic Monte Carlo, *Phys. Procedia* **6**, 95 (2010).
- [25] J. Carlström, Spin-charge transformation of lattice fermion models: Duality approach for diagrammatic simulation of strongly correlated systems, *J. Phys.: Condens. Matter* **29**, 385602 (2017).
- [26] J. Carlström, Diagrammatic Monte Carlo procedure for the spin-charge transformed Hubbard model, *Phys. Rev. B* **97**, 075119 (2018).
- [27] J. Carlström, Spectral shift technique for strongly correlated lattice fermions, [arXiv:2111.05877](https://arxiv.org/abs/2111.05877).
- [28] J. Carlström, *In situ* controllable magnetic phases in doped twisted bilayer transition metal dichalcogenides, *Phys. Rev. Res.* **4**, 043126 (2022).
- [29] O. Goulko, A. S. Mishchenko, L. Pollet, N. Prokof'ev, and B. Svistunov, Numerical analytic continuation: Answers to well-posed questions, *Phys. Rev. B* **95**, 014102 (2017).